



# ADVANCES IN FOREST FIRE RESEARCH 2018

EDITED BY

**DOMINGOS XAVIER VIEGAS**  
ADAI/CEIF, UNIVERSITY OF COIMBRA, PORTUGAL

# The effect of interstitial flow on the burning dynamics of porous fuel beds

Zakary Campbell-Lochrie<sup>1\*</sup>; Carlos Walker-Rávena<sup>1</sup>; Eric V. Mueller<sup>1</sup>; Rory M. Hadden<sup>1</sup>

<sup>1\*</sup>University of Edinburgh, Edinburgh, {Z.Campbell.Lochrie@ed.ac.uk}

## Abstract

The effect of fuel bed structure on the processes controlling flame spread in porous media is investigated. The fuel loading and bulk density of Pine needle (*Pinus taeda x rigida*) fuel beds was varied resulting in changes in the fuel bed porosity. Experiments were conducted in no slope, quiescent conditions on a 1.5 m long flame spread table, which was instrumented at three locations to determine gas phase temperature and airflow. Flame height, heat release rate and burning rate were also measured.

Increases in overall fuel loading or decreases in bulk density resulted in increasing flame spread rate, flame height and HRR. At the highest fuel loading (0.8 kg/m<sup>2</sup>) the spread rate for the lowest bulk density case (10 kg/m<sup>3</sup>) was 180 mm/min compared to 88 mm/min in the highest bulk density case (40 kg/m<sup>3</sup>), while a linear increase ( $R^2 = 0.97$ ) in flame spread rate as a function of fuel bed porosity was also observed. The magnitude of the entrainment flow towards the approaching flame front is shown to increase with porosity, from 0.4 m/s (94.5 % porosity) to 0.9 m/s (98.6 % porosity), at 0.8 kg/m<sup>2</sup> fuel loading. An increase in the flow magnitude was also observed with increases in fuel loading for bulk densities of 10 kg/m<sup>3</sup>, but not for bulk densities of 20 kg/m<sup>3</sup>. At the higher bulk density, the effect of the increased fuel loading on the buoyancy-induced entrainment appears to be limited by porosity, resulting in reduced convective cooling ahead of the flame front, alongside the expected changes in radiation attenuation as the fuel bed depth varies.

**Keywords:** Flame Spread, Porous Fuel, Porosity, Flow

## 1. Introduction

The litter layer represents an important fuel stratum in wildland environments, and it has a significant role in surface flame spread. The physical phenomena involved in surface flame spread have been extensively studied (Catchpole *et al.* 1998; Wotton *et al.* 1999; Marcelli *et al.* 2004) however, the processes which control this require further exploration.

Existing, laboratory and field scale, flame spread studies have shown that flame spread is influenced by the weather conditions (wind, humidity), topography and fuel. The first two categories have been investigated in several previous laboratory scale flame spread experiments in natural porous fuel beds, involving a range of external flow conditions and slope angles (Mendes-Lopes *et al.* 2003; Liu *et al.* 2014; Rossa *et al.* 2015). To date, relatively few studies have systematically investigated the effect of the fuel bed properties on the physical processes driving flame spread (Simeoni *et al.* 2011; Finney *et al.* 2013).

Given the porous nature of natural fuel beds, flame spread is often modelled using a solid-gas multi-phase approach (Grishin 1996; Sullivan 2009). Improvement of these models requires characterisation of multiple factors such as chemical, thermophysical and geometrical properties (Balbi *et al.* 2014) to allow development of improved sub-models.

These geometrical properties can be described at multiple scales, and encompass global fuel bed structural parameters (bulk density, porosity), local structural variations (fuel element interactions, needle orientation), and individual fuel element properties (density, surface to volume ratio).

Previous studies have shown a relationship between bulk density and fuel loading, and the flame spread rate (Morandini *et al.* 2013; Balbi *et al.* 2014). In these studies, often only the effect of fuel

loading is studied, or, if studied, the bulk density is typically altered by changing the fuel loading. These parameters are related and changing the bulk density in this way does not allow explicit consideration of the fuel bed porosity to be independently investigated. In this study, the bulk density is controlled by altering the average height of the fuel bed, enabling fuel beds of multiple bulk densities to be investigated for any given fuel loading.

There has been little previous work to describe the effect of fuel bed characteristics on the physical mechanisms governing these variations in fire behaviour. Previous authors have used engineered materials to investigate the effect of structure within porous fuel beds (Wolff *et al.* 1991; Finney *et al.* 2013) however there remains a need to investigate the effect of structural changes within natural fuel beds on the observed variations in fire behaviour (flame spread rate, flame height, HRR) and the physical processes responsible.

## 2. Experimental Methods

### 2.1. Experimental Setup

A series of laboratory scale flame spread experiments were undertaken, involving pine needle fuel beds on a 1.5 m x 0.67 m flame spread table. The table consisted of adjustable steel side walls, and a vermiculite substrate base instrumented at three measurement locations (0.5 m, 0.8 m and 1.1 m from the ignition line) as shown in Figure .

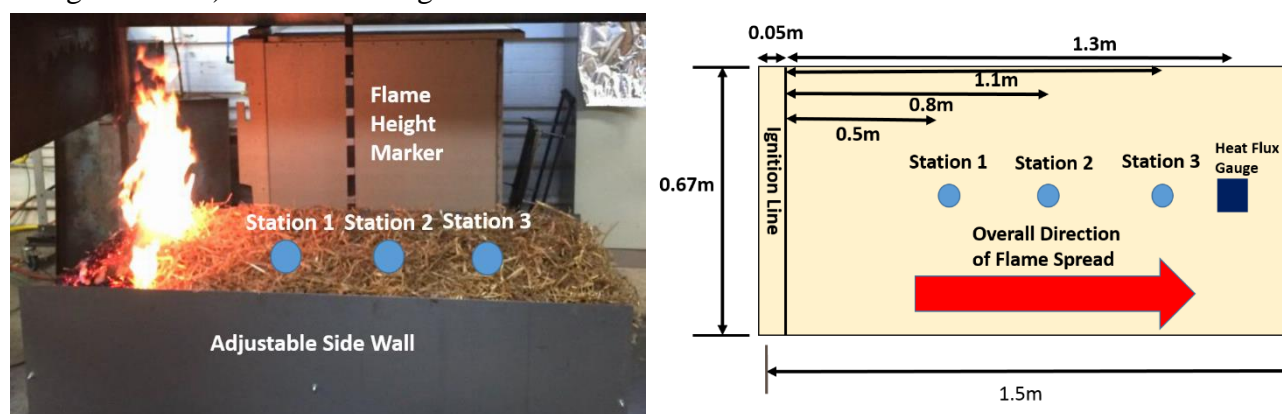


Figure 1 - Photo and diagram of experimental setup including 3 measurement station locations

Each measurement location consisted of a gas phase thermocouple (0.25 mm thick, K Type) 10 mm above the base; and a bi-directional pressure probe (McCaffrey and Heskestad 1976) with the centre axis located 10 mm above the vermiculite base. The gas phase thermocouples are used to calculate the flame spread rate, and in conjunction with the pressure probe measurements, the in-bed flow velocity.

Additionally, a water-cooled heat flux gauge was positioned flush to the upper surface of the vermiculite (bottom of fuel bed), at a distance of 1.3 m from the ignition line, to measure the total incident heat flux. The thermocouple, pressure probe, and heat flux gauge data were logged at 10 Hz.

Experiments were filmed, with flame height and bed length markers allowing the flame height and spread rate to be determined through video analysis. The table was placed on a load cell to record the burning rate. The HRR was measured by oxygen consumption calorimetry (Janssens 1991).

All experiments were ignited using alumina-silica fibre (0.67 m x 0.05 m) soaked in 10 ml of acetone. The flameout time was defined as the time at which visible flaming was no longer observed within the fuel bed.

## 2.2. Fuel Properties

### 2.2.1. Pine Needle Properties

Dead *Pinus taeda x rigida* (Loblolly - Pitch Pine hybrid) needles were collected in November 2017 from the Silas Little Experimental Forest in New Lisbon, New Jersey. Needles were stored indoors at ambient conditions and were otherwise unconditioned prior to use. The Fuel Moisture Content (FMC) of the pine needles was measured for each experiment, by oven drying needle samples for 24 hours at 60 °C.

The geometrical properties were measured through random sampling. A needle density of 725 kg/m<sup>3</sup> [10/0.12], diameter of 1.34 mm [25/0.12], and surface to volume ratio of 4899 m<sup>-1</sup> [25/446] were calculated [N/ Std. Dev.].

### 2.2.2. Fuel Bed Construction

The construction of the fuel beds followed a set procedure to ensure consistency. Unconditioned pine needles were weighed on a precision balance, and then distributed within ten equal sections of the table, to ensure uniformity of fuel loading. Within each of these sections, needles were dropped randomly on to the table with no effort to control the position or orientation of individual needles.

The height of the adjustable sidewalls was set relative to the average height of the fuel bed providing an identical edge condition in each case. The walls extended 0.03 m above the fuel bed preventing lateral entrainment within the fuel bed. This has been shown to result in a more linear flame front (Liu et al. 2015).

The bulk density was varied by altering the average height of the fuel bed. This allowed different bulk densities to be tested, at the same overall fuel loading. The fuel bed heights studied across the various fuel loadings, ranged from 0.01 m to 0.08 m.

## 2.3. Fire Behaviour Measurements

The spread rate was calculated using the gas phase temperature measurements, which are characterised by an initial pre-heating period, followed by a large temperature spike. The flame arrival time was defined as the initial time at which the temperature exceeds 300 °C, with the interval between successive arrival times used to calculate the spread rate.

The mass was measured across the duration of the experiment using a balance with accuracy of ± 0.001 kg. The quasi-steady mass loss rate was calculated using a 5 s moving average. The HRR was calculated, through oxygen consumption calorimetry (Janssens 1991), with the peak HRR also reported for each experiment.

The flame height was determined through video analysis, with a vertical length scale (0.05 m divisions) positioned at each measurement location. The flame heights were based on the upper extent of the continuous flame region.

## 3. Results and Discussion

### 3.1. Flame Height, Flame Spread and Heat Release Rate Observations

The effect of changes in global fuel bed structural characteristics is illustrated in Figure 2. This is a composite image of an experiment that involved a graduated fuel bed composed of four successive areas of both differing fuel loading and bulk density. For a change in fuel loading of 1.6 kg/m<sup>2</sup> to 0.2 kg/m<sup>2</sup> the flame height was observed to reduce from (0.9 ± 0.03) m to (0.05 ± 0.03) m. The fire line intensity also decreased from 75 kWm<sup>-1</sup> to 9 kWm<sup>-1</sup>.

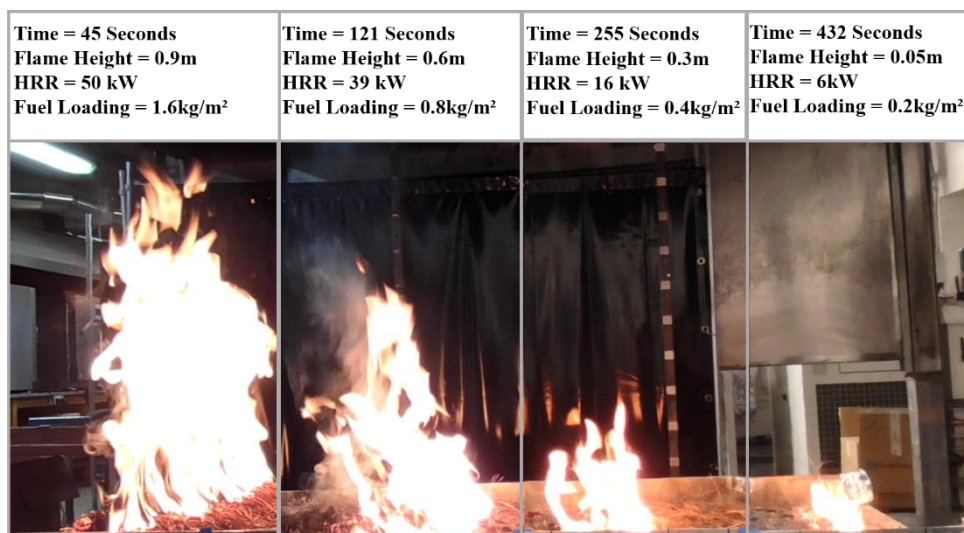


Figure 2 - Time lapsed photo of graduated fuel bed with burning characteristics at each segment centreline

These effects are in agreement with the trends observed in similar previous studies (Morandini *et al.* 2013) where simultaneous changes in fuel loading and bulk density led to increasing flame height, HRR and spread rate. Experiments of this nature, where both fuel loading and bulk density are simultaneously varied, are common, however previous studies (Simeoni *et al.* 2011; Santoni *et al.* 2014) have indicated that both these characteristics influence combustion dynamics and fire behaviour.

In this study, these fuel bed characteristics were therefore investigated separately through a series of experiments involving fuel beds of varying height, across a range of fuel loadings. The results from these experiments, including the average values of flame spread rate, peak HRR, mass loss rate, and flame height are summarised in Table .

Sustained flaming and flame spread were not observed at fuel loadings of 0.2 kg/m<sup>2</sup> at either bulk density investigated. This suggests that the small-scale structure of needles may be playing a significant role at low fuel loadings.

Table 1 - Effect of fuel loading and bulk density on fire behaviour for *P. taeda x rigida* hybrid fuel beds

Fuel Loading (Wet Mass) (kg/m <sup>2</sup> )	Bulk Density (kg/m <sup>3</sup> )	Porosity (% Wet)	Average Fuel Bed Height (m)	Average Moisture Content (% Dry Basis)	Average Flame Spread Rate (mm/min)	Peak Heat Release Rate (kW)	Quasi Steady Mass Loss Rate (g/s)	Average Flame Height (m ± 0.025)
0.2	20	97.2	0.01	16.4	Auto-Extinguished	-	-	-
0.2	10	98.6	0.02	16.4	Auto-Extinguished	-	-	-
0.4	20	97.2	0.02	15.5	96 ± 3	10 ± 1	0.4 ± 0.2	0.1
0.4	10	98.6	0.04	15.2	129 ± 21	17 ± 3	0.4 ± 0.2	0.2
0.6	20	97.2	0.03	15.2	132 ± 12	18 ± 0.5	0.8 ± 0.2	0.3
0.6	10	98.6	0.06	15.6	168 ± 3	24 ± 1	1.8 ± 0.2	0.4
0.8	40	94.5	0.02	16.1	88 ± 7	17 ± 1	0.7 ± 0.05	0.3
0.8	20	97.2	0.04	15.7	134 ± 12	23 ± 1	1.0 ± 0.2	0.4
0.8	11.4	98.4	0.07	17.4	177 ± 3	34 ± 0.5	1.7 ± 0.2	0.5
0.8	10	98.6	0.08	15.9	180 ± 3	35 ± 0.5	1.4 ± 0.2	0.5

For the cases of fuel loading of 0.4 kg/m<sup>2</sup> and above, sustained flame spread was observed. It was observed that an initial increase in fuel loading or a decrease in bulk density resulted in increased HRR, mass loss rate, flame height and spread rate. At greater fuel loadings (0.8 kg/m<sup>2</sup>), the mass loss rate at 10 kg/m<sup>3</sup> reduced to 1.4 ± 0.2 g/s, compared to 1.8 ± 0.2 g/s, for the 0.6 kg/m<sup>2</sup>, 10 kg/m<sup>3</sup> case. Increasing the bulk density always resulted in a decrease in the spread rate. Increasing bulk density also resulted in increased burning rate except at the lowest fuel loading of 0.4 kg/m<sup>2</sup> where there was no variation although this may be as a result of the mass loss resolution.

### 3.2. Effect of Global Structural Changes on Porosity

It is hypothesised that these changes in fire behaviour, and the sensitivity to bulk density, arise due to changes in the processes occurring within the fuel bed. Altering the global structural characteristics of the fuel bed should result in changes in both the permeability and porosity of the fuel bed, which may then alter the in-bed flow behaviour.

The effect of fuel loading and bulk density changes can be characterised in terms of the porosity (or gaseous volume fraction,  $\alpha_g$ ), of the fuel bed which is given by,

$$\alpha_g = 1 - \alpha_s \tag{1}$$

$$\alpha_s = \rho^* / \rho \tag{2}$$

Where  $\alpha_s$  is the solid volume fraction,  $\rho^*$  is the bulk density and,  $\rho$  is the particle density of the pine needles. Figure 3 presents the flame spread rate as a function of the fuel bed porosity for the 0.8 kg/m<sup>2</sup> fuel loading. A linear increase ( $R^2 = 0.97$ ) in flame spread rate as a function of increasing porosity is observed. This indicates that the burning dynamics are strongly influenced by porosity but does not indicate the physical mechanisms responsible for these changes.

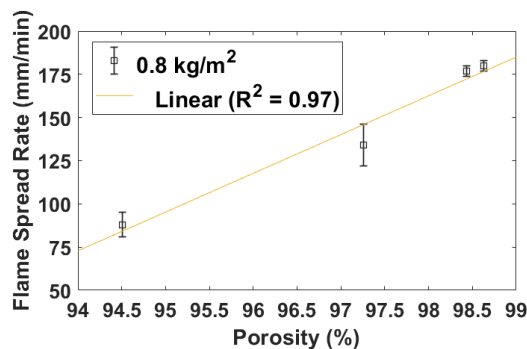


Figure 3 - Relationship between the average flame spread rate and porosity at 0.8 kg/m<sup>2</sup> fuel loading

### 3.3. Heat Transfer Mechanisms

The radiative heat transfer from the flame to the bottom of the fuel bed is influenced by the characteristics of the flame (flame length and tilt angle) (Morandini *et al.* 2001) and of the fuel bed (bulk density, particle size, and permeability) (Simeoni *et al.* 2012).

Past studies have shown both theoretically (De Mestre *et al.* 1989; Vaz *et al.* 2004a) and experimentally (Butler 1993; Vaz *et al.* 2004b) that increased fuel bed bulk density, and hence reduced porosity, results in increased radiation attenuation. As the porosity was changed by increasing the fuel bed height however then the depth of the absorbing media will also increase. This will reduce the effect of the extinction coefficient as the porosity is increased.

An increase in flame height (as observed to occur with increasing porosity) results in increased emittance of heat flux from the flame. As the fuel bed porosity is increased then it would therefore be expected that a greater heating period ahead of the flame front arrival would be observed.

Measurement of the total incident heat flux to the bottom of the fuel bed however indicates a decrease in the duration of the pre-heating period, ahead of the flame front arrival, as the porosity is increased. As shown in Figure 4 (a) the time period before flame arrival in which a non-zero heat flux is observed decreases with decreasing bulk density, from 42 s at 40 kg/m<sup>3</sup> bulk density (94.51 % porosity), to 13 s at 10 kg/m<sup>3</sup> bulk density (98.63 % porosity). The same trend is also observed (Figure 4(b)) if the total heat flux is calculated relative to the position of the flame front from the measurement location (d = 0), to account for the difference in spread rate.

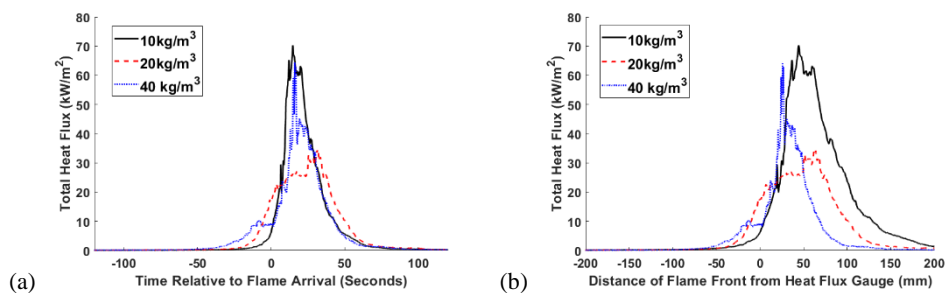


Figure 4 - Total incident heat flux to bottom surface of the fuel bed, for a range of bulk densities at a fuel load of 0.8 kg/m<sup>2</sup> relative to (a) time of flame arrival (b) flame front distance from the heat flux gauge

The total incident heat flux for fuel beds of varying fuel loading at a constant bulk density of 10 kg/m<sup>3</sup>, showed an earlier initial increase in heat flux at lower fuel loadings, as shown in Figure 5. In this case the flame height increases for higher fuel loadings, but the attenuation also increases as the fuel bed depth grows with a constant extinction coefficient. For the same range of fuel loadings at a higher bulk density (20 kg/m<sup>3</sup>) however this trend in the heat flux onset is no longer observed.

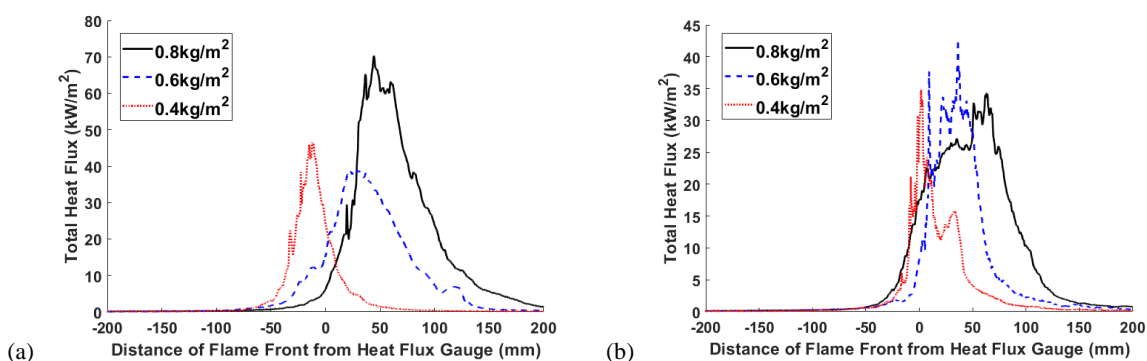


Figure 5 - Total incident heat flux to the bottom surface of the fuel bed for a range of fuel loadings at a bulk density of (a) 10 kg/m<sup>3</sup> and (b) 20 kg/m<sup>3</sup>

The total heat flux to the bottom of the fuel bed also includes the effects of convective heat transfer in addition to the radiative heat transfer. This can include natural convection as well as flame-induced convection (Liu *et al.* 2015) driven by entrainment from the buoyant plume. Characterisation of the flow profile within the fuel bed is required to understand the influence of this buoyancy driven entrainment.

### 3.4. In-Bed Flow Behaviour

The flow data were derived from pressure measurements and processed using a Local Polynomial Regression Method (LOESS) (Cleveland 1979), with a 1 s window. The flow velocity is plotted relative to the distance between the flame front and the pressure probe (d = 0), with a negative distance indicating an approaching flame front.

The variability in flow velocity trends was assessed through comparison of the velocity data from three repeats of an identical case (0.8 kg/m<sup>2</sup> fuel loading, 40 kg/m<sup>3</sup> bulk density), as shown in Figure

6. Flow data was recorded prior to ignition to provide an average value at the time of ignition, the largest standard deviation in this averaged zero value was 0.11 m/s. The greatest discrepancy in the peak entrainment towards the approaching flame front was 0.13 m/s.

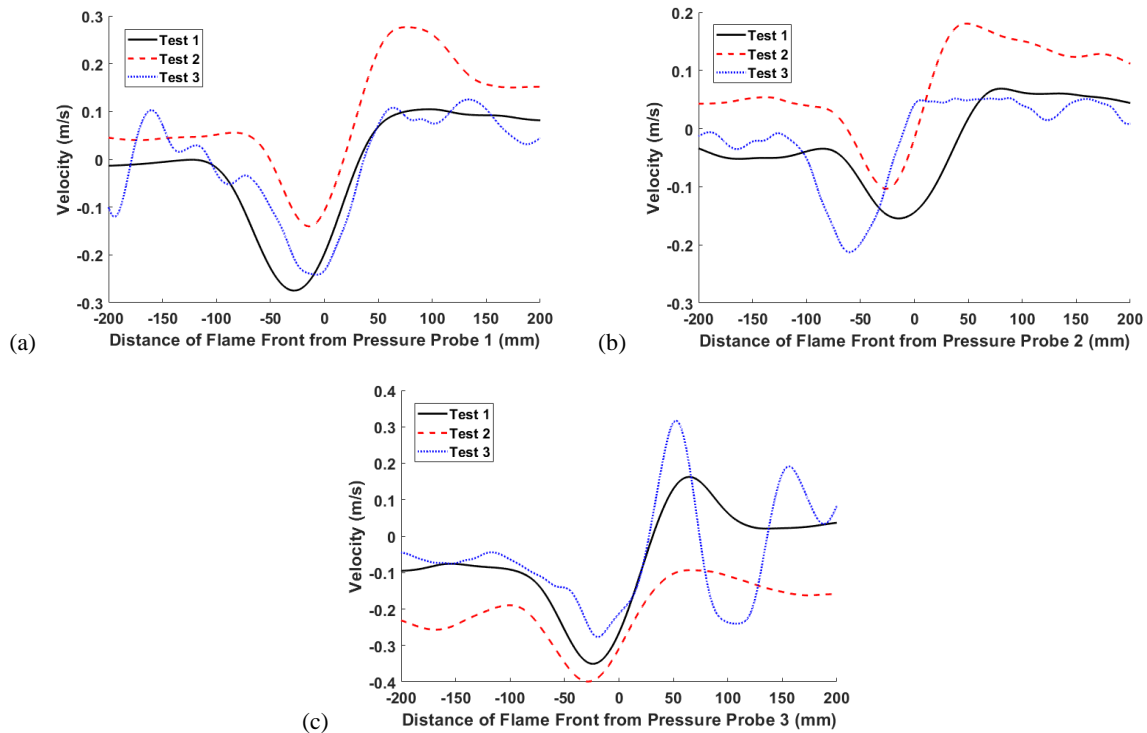
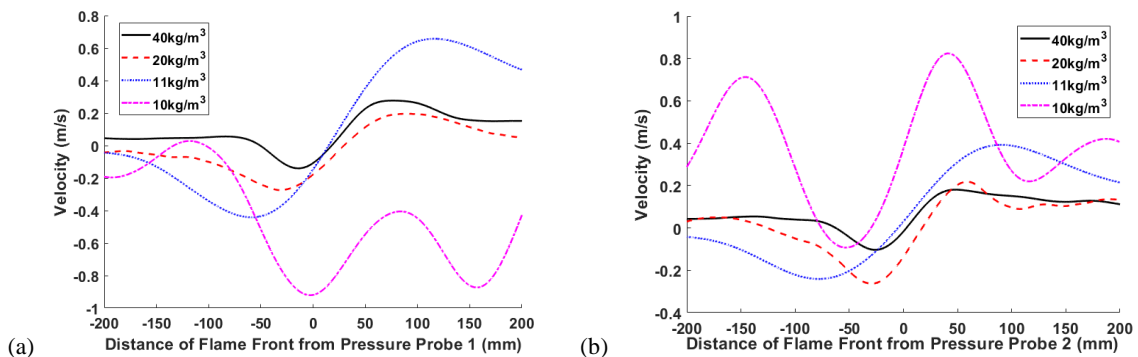


Figure 6 - In-bed flow velocity relative to flame front distance from (a) Probe 1, (b) Probe 2, (c) Probe 3, for three repeats of an identical case ( $0.8 \text{ kg/m}^2$  fuel loading,  $40 \text{ kg/m}^3$  bulk density)

The in-bed flow velocity trends are generally characterised by a period of entrainment (indicated by negative velocities) prior to the arrival of the flame front, followed by a period of flow concurrent with the flame spread direction after the arrival of the flame front. In general, lower bulk densities do not follow this trend, as shown in Figure 7. It is suggested that this is due to the relatively high porosity allowing small-scale variation in needle structure to be more significant. The peak magnitude of the pre-flame arrival entrainment velocity is observed to increase, with decreasing bulk density (increasing porosity), with a peak value of  $0.4 \text{ m/s}$  for the  $40 \text{ kg/m}^2$  case, and  $0.9 \text{ m/s}$  for the  $10 \text{ kg/m}^2$  case.



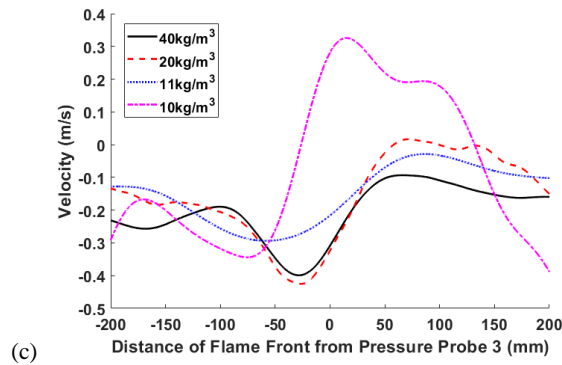


Figure 7 - In-bed flow velocity relative to flame front distance from pressure probes at (a) 0.5m (b) 0.8m and (c) 1.1m from the ignition line, for a range of bulk density (40, 20, 11, 10) kg/m<sup>3</sup>, at 0.8 kg/m<sup>2</sup> fuel load

The increase in the pre-flame arrival entrainment velocity with reducing bulk density will result in a greater entrainment of ambient air, through the fuel bed, towards the fire front. The increased ambient airflow at the bottom of the fuel bed will result in convective cooling resulting in a reduced pre-heating period ahead of the flame front, as observed in the heat flux data.

Comparison of the in-bed flow velocity profiles for a range of fuel loadings, at a constant bulk density (10 kg/m<sup>3</sup>), reveals a similar, but less consistent trend, as shown in Figure .

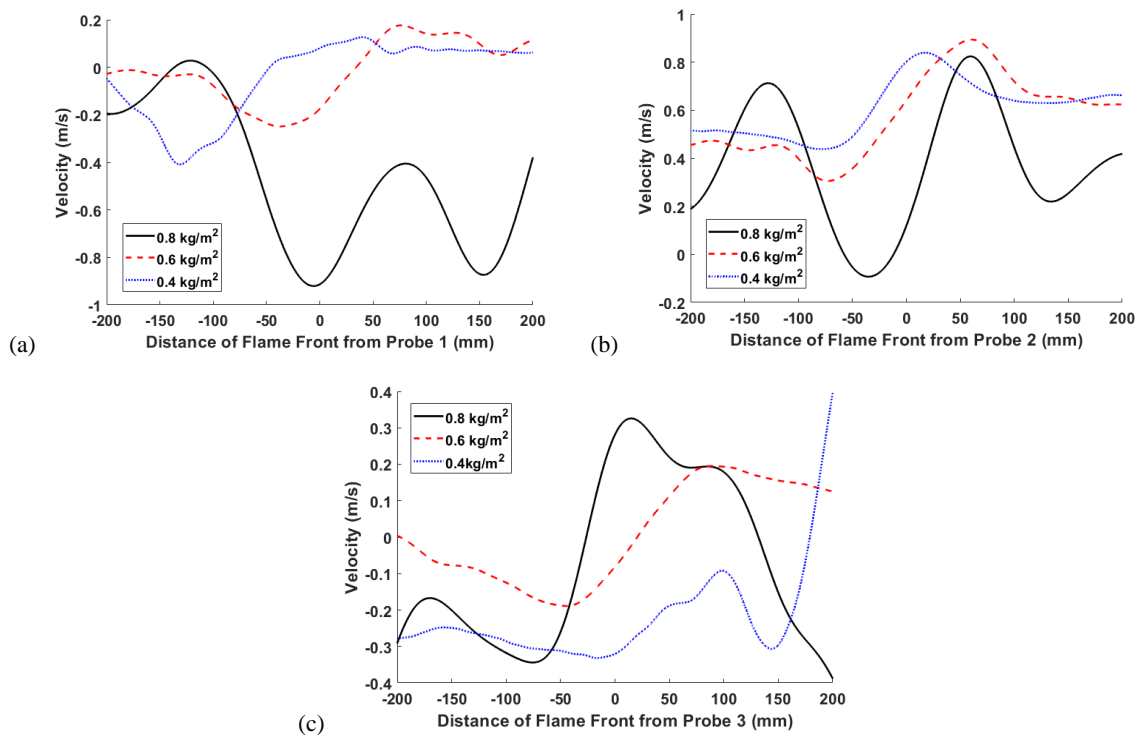


Figure 8 - In-bed flow velocity relative to flame front distance from pressure probes at (a) 0.5 m (b) 0.8 m and (c) 1.1m from the ignition line, for a range of fuel loads (0.8, 0.6, 0.4) kg/m<sup>2</sup>, at 10kg/m<sup>3</sup> bulk density

As shown in Figure 9 however, at a bulk density of 20 kg/m<sup>2</sup> the flow magnitude displays no clear trend with fuel loading. At the lowest fuel loading (0.4 kg/m<sup>2</sup>), the high entrainment velocity at probe 3 may be due to the relative importance of the small-scale variations in permeability, as the fuel bed height (0.02 m) is equal to the height of the pressure probe.

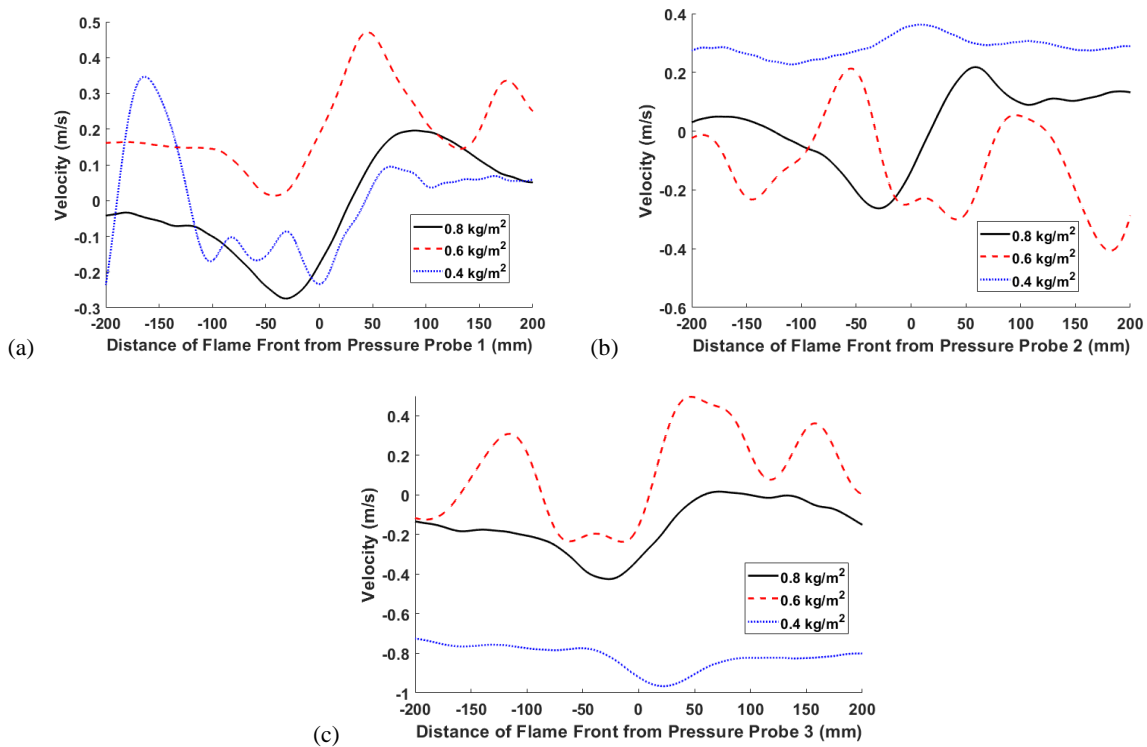


Figure 9 - In-bed flow velocity relative to flame front distance from pressure probes at (a) 0.5 m (b) 0.8 m and (c) 1.1 m from the ignition line, for a range of fuel loads (0.8, 0.6, 0.4) kg/m<sup>2</sup> at 20 kg/m<sup>3</sup> bulk density

The reduced effect of fuel loading on the entrainment velocity is in accordance with the lack of variation in the initial rise in total heat flux. This suggests that the fuel bed porosity in this case is limiting the effect of fuel loading increases on the entrainment flow magnitude.

#### 4. Conclusions

Flame spread experiments for pine needle fuel beds of varying fuel bed height show that independent changes in either the fuel loading or the bulk density leads to observable changes in fire behaviour, with a strong coupling between burning behaviour and fuel bed porosity.

These changes in overall fuel bed porosity are observed to result in changes in the heat transfer mechanisms within the fuel bed. As the entrainment flow velocity increases with reducing bulk density, the onset of heating to the bottom of the fuel bed is delayed relative to flame arrival time. For the 0.8 kg/m<sup>2</sup> case, the initial rise in total heat incident flux at the bottom of the fuel bed was observed at 42 s before the flame arrival for a bulk density of 40 kg/m<sup>3</sup>, compared to 13 s before flame arrival for a bulk density of 10 kg/m<sup>3</sup>. This delay is also observed across varying fuel loadings at 10 kg/m<sup>3</sup> but not at 20 kg/m<sup>3</sup> bulk density.

The peak magnitude of the entrainment velocity, through the unburnt fuel, towards the approaching flame front, was observed to increase, with decreasing bulk density with a peak value of 0.4 m/s for the 40 kg/m<sup>3</sup> bulk density (94.5 % porosity) case, and 0.9 m/s for the 10 kg/m<sup>3</sup> bulk density (98.6 % porosity) case. Increasing the fuel loading for 10 kg/m<sup>3</sup> fuel loadings led to similar increase in entrainment flow, however little trend was observed in the 20 kg/m<sup>3</sup> cases. This suggests that although the buoyancy is entrainment driven, it is limited by the porosity in the 20 kg/m<sup>3</sup> case. This highlights the importance of both the fuel loading and the structural properties of the fuel bed on the physical mechanisms within the fuel bed, and the need for a greater understanding of the effect on the overall burning characteristics.

## 5. Acknowledgements

The authors wish to thank the Strategic Environmental Research and Development Program (SERDP) for their financial support under the project grant RC-2641. The authors would also like to thank Dr Michael Gallagher for providing the fuels used in this study, and Hugo Rouvrais for his assistance during the experiments.

## 6. References

- Balbi J-H, Viegas DX, Rossa C, Rossi J-L, Chatelon F-J, Cancellieri D, Simeoni A, Marcelli T (2014) Surface Fires: No Wind, No Slope, Marginal Burning. *Journal of Environmental Science and Engineering A* **3**, 73–86.
- Butler B (1993) Experimental measurements of radiant heat fluxes from simulated wildfire flames. In ‘Proc. 12th Conf. Fire For. Meteorol.’, 104–111
- Catchpole WR, Catchpole EA, Butler BW, Rothermel RC, Morris GA, Latham DJ (1998) Rate of spread of free-burning fires in woody fuels in a wind tunnel. *Combustion Science and Technology* **131**, 1–37. doi:10.1080/00102209808935753.
- Cleveland WS (1979) Robust locally weighted regression and smoothing scatterplots. *Journal of the American Statistical Association* **74**, 829–836. doi:10.1080/01621459.1979.10481038.
- Finney MA, Forthofer J, Grenfell IC, Adam BA, Akafuah NK, Saito K (2013) A study of flame spread in engineered cardboard fuelbeds: Part I: Correlations and observations. In ‘Proc. Seventh Int. Symp. Scale Model.’,
- Grishin AM (1996) General mathematical model for forest fires and its applications. *Combustion, Explosion and Shock Waves* **32**, 503–519. doi:10.1007/BF01998573.
- Janssens ML (1991) Measuring rate of heat release by oxygen consumption. *Fire Technology* **27**, 234–249. doi:10.1007/BF01038449.
- Liu N, Wu J, Chen H, Xie X, Zhang L, Yao B, Zhu J, Shan Y (2014) Effect of slope on spread of a linear flame front over a pine needle fuel bed: Experiments and modelling. *International Journal of Wildland Fire* **23**, 1087–1096. doi:10.1071/WF12189.
- Liu N, Wu J, Chen H, Zhang L, Deng Z, Satoh K, Viegas DX, Raposo JR (2015) Upslope spread of a linear flame front over a pine needle fuel bed: The role of convection cooling. *Proceedings of the Combustion Institute* **35**, 2691–2698. doi:10.1016/j.proci.2014.05.100.
- Marcelli T, Santoni PA, Simeoni A, Leoni E, Porterie B (2004) Fire spread across pine needle fuel beds: Characterization of temperature and velocity distributions within the fire plume. *International Journal of Wildland Fire*. doi:10.1071/WF02065.
- McCaffrey BJ, Heskestad G (1976) A robust bidirectional low-velocity probe for flame and fire application. *Combustion and Flame*. doi:10.1016/0010-2180(76)90062-6.
- Mendes-Lopes JMC, Ventura JMP, Amaral JMP (2003) Flame characteristics, temperature-time curves, and rate of spread in fires propagating in a bed of *Pinus pinaster* needles. *International Journal of Wildland Fire* **12**, 67–84. doi:10.1071/WF02063.
- De Mestre NJ, Catchpole EA, Anderson DH, Rothermel RC (1989) Uniform Propagation of a Planar Fire front Without Wind. *Combustion Science and Technology* **65**, 231–244. doi:10.1080/00102208908924051.
- Morandini F, Perez-Ramirez Y, Tihay V, Santoni PA, Barboni T (2013) Radiant, convective and heat release characterization of vegetation fire. *International Journal of Thermal Sciences* **70**, 83–91. doi:10.1016/j.ijthermalsci.2013.03.011.

- Morandini F, Santoni PA, Balbi JH (2001) The contribution of radiant heat transfer to laboratory-scale fire spread under the influences of wind and slope. *Fire Safety Journal* **36**, 519–543. doi:10.1016/S0379-7112(00)00064-3.
- Rossa CG, Davim DA, Viegas DX (2015) Behaviour of slope and wind backing fires. *International Journal of Wildland Fire* **24**, 1085–1097. doi:10.1071/WF14215.
- Santoni PA, Bartoli P, Simeoni A, Torero JL (2014) Bulk and particle properties of pine needle fuel beds – influence on combustion. *Int. J. Wildl. Fire* **23**, 1076–1086. doi:10.1071/WF13079.
- Simeoni A, Bartoli P, Torero JL, Santoni PA (2011) On the role of bulk properties and fuel species on the burning dynamics of pine forest litters. In ‘Fire Saf. Sci.’, doi:10.3801/IAFSS.FSS.10-1401.
- Simeoni A, Thomas JC, Bartoli P, Borowieck P, Reszka P, Colella F, Santoni PA, Torero JL (2012) Flammability studies for wildland and wildland-urban interface fires applied to pine needles and solid polymers. *Fire Safety Journal* **54**, 203–217. doi:10.1016/j.firesaf.2012.08.005.
- Sullivan AL (2009) Wildland surface fire spread modelling, 1990–2007. 1: Physical and quasi-physical models. *International Journal of Wildland Fire* **18**, 349–368. doi:10.1071/WF06144.
- Vaz GC, André JCS, Viegas DX (2004a) Fire spread model for a linear front in a horizontal solid porous fuel bed in still air. *Combustion Science and Technology* **176**, 135–182. doi:10.1080/00102200490255343.
- Vaz GC, André JCS, Viegas DX (2004b) Estimation of the radiation extinction coefficient of natural fuel beds. *International Journal of Wildland Fire* **13**, 65–71. doi:10.1071/WF03009.
- Wolff MF, Carrier GF, Fendell FE (1991) Wind-Aided Firespread Across Arrays of Discrete Fuel Elements. II. Experiment. *Combustion Science and Technology* **77**, 261–289. doi:10.1080/00102209108951731.
- Wotton BM, McAlpine RS, Hobbs MW (1999) The effect of fire front width on surface fire behaviour. *International Journal of Wildland Fire* **9**, 247–253. doi:10.1071/WF00021.